Journal of Power Sources 208 (2012) 24–34

Contents lists available at SciVerse ScienceDirect

Journal of Power Sources

journal homepage: www.elsevier.com/locate/jpowsour

Direct two-dimensional electrochemical impedance spectra simulation for solid oxide fuel cell

Yixiang Shi*, Hongjian Wang, Ningsheng Cai

Key Laboratory for Thermal Science and Power Engineering of Ministry of Education, Tsinghua University, Beijing 100084, China

ARTICLE INFO

Article history:
Received 7 December 2011
Received in revised form 3 February 2012
Accepted 4 February 2012
Available online 14 February 2012

Keywords:
Solid oxide fuel cell
Electrochemical impedance spectra
Modeling
Local impedance
Electro-thermal effect

ABSTRACT

A two-dimensional (2D) EIS simulation approach is developed by solving a SOFC unit cell model with imposed sinusoidal voltage perturbations at different frequencies. The transient SOFC unit cell model describes the intricate interdependency among the ionic/electronic conduction, multi-component species transport, electrochemical reaction processes and electrode microstructure as well as the coupling processes of mass, energy, momentum transport within flow channels. The model calculates the local transient response and impedance spectra as a function of channel position. The effects of the reaction depletion, product accumulation as well as the temperature variation along the flow channels on the EIS spectra are numerically simulated with a counter-flow mode. The results show that the convection-diffusion process along the flow channel has significant effects on the low frequency half circle of the impedance spectra. The temperature oscillations accumulate along the flow channels, and then affect the current responses which probably lead to an electro-thermal impedance effects.

1. Introduction

Electrochemical Impedance Spectroscopy (EIS) is a widely used characterization method to distinguish processes occurring on different time-scales and gain insights into limiting factors limiting of the solid oxide fuel cell performance.

Several researchers have developed or are currently developing SOFC impedance models. Fleig and Maier [1] studied the influence of imperfect contact between porous electrodes on the impedance by using finite elements modeling. Bieberle and Gauckler [2] developed a physicochemical model to describe the detailed elementary electrochemical reactions within the electrode. To simulate the electrochemical impedance spectra, the models were solved directly through the State Space Modeling (SSM) approach, which is widely used in control theory for solving complex differential equations. Bessler [3] presented a new computational method for calculating the impedance based on detailed physicochemical models. The method was based on numerical simulations of the transient behavior of the reaction system. The impedance was then calculated in the time domain from the simulated periodic response of the system, maintaining its full nonlinear response. Zhu and Kee [4] developed a time-accurate model to analyze EIS spectra in anode-supported button cells with internal methane reforming. A common feature of all these modeling approaches is the assumption of in-plane uniformity which could simplify the system to one dimension in the electrode thickness direction.

However, Schneider et al. [5,6] found that the second loop of impedance can be related with the propagation of the oscillation of product concentration along the flow channel, and they experimentally verified the existence of the two-dimensional effects, and thus the current response in upstream parts of the cell affects the impedance response in downstream regions.

This paper contributes a two-dimensional (2D) EIS simulation approach by solving a SOFC unit cell transient model with imposed sinusoidal voltage perturbations at different frequencies. The transient SOFC unit cell model described the intricate interdependency among the ionic conduction, electronic conduction, multi-component species transport, electrochemical reaction processes and electrode microstructure within Membrane-Electrode-Assembly (MEA) as well as the coupling processes of mass, energy, momentum transport and charge transfer within flow channel and inter-connectors. Then, the effects of the reaction depletion, product accumulation as well as the temperature variation along the flow channels on the EIS spectra was numerically simulated at counter-flow operation mode for the SOFC unit cell.

2. Model development

2.1. Model assumptions and calculation domain

Numerical models of planar SOFC were developed by coupling governing equations of charge, mass, momentum, energy

* Corresponding author. Tel.: +86 10 62789955; fax: +86 10 62770209.
E-mail address: shyx@tsinghua.edu.cn (Y. Shi).

0378-7753/$ – see front matter © 2012 Elsevier B.V. All rights reserved.
doi:10.1016/j.jpowsour.2012.02.012

Nomenclature

c	concentration ($mol\,m^{-3}$)
C	specific double layer capacitance ($F\,m^{-2}$)
D	diffusion coefficient ($m^2\,s^{-1}$)
E	activation energy ($J\,mol^{-1}$)
F	frequency (Hz)
I	current (A)
i	current density ($A\,m^{-2}$)
i_0	exchange current density ($A\,m^{-2}$)
M_i	molecular weight of species i ($kg\,mol^{-1}$)
P	pressure (Pa)
Q	source term of charge balance equations ($A\,m^{-3}$)
R	gas constant ($8.314\,J\,mol^{-1}\,K^{-1}$)
R_i	source term of mass balance equations ($kg\,m^{-3}\,s^{-1}$)
S_{TPB}	active surface area per unit volume ($m^2\,m^{-3}$)
L_{TPB}	active length per unit volume ($m\,m^{-3}$)
t	time (s)
T	temperature (K)
V	electric potential or cell voltage (V)
V_i,V_j	diffusion volume
w_i	mass fraction of species i
x_k	molar fraction of gas-phase species k
Y	admittance (S)
Z	coordination number

Greek letters

α	transfer coefficient
β	tuning parameter ($\Omega^{-1}\,m^{-2}$)
ε	porosity
η	overpotential (V)
ρ	density ($kg\,m^{-3}$)
σ	conductivity ($S\,m^{-1}$)
τ	tortuosity
ω	angle frequency ($rad\,s^{-1}$)

Superscripts

eff	effective

Subscripts

ac	anode chamber
act	activation/active
an	anode
avg	average
bulk	bulk phase
ca	cathode
cc	cathode chamber
elec	electronic
F	Faraday
inter	interface
ion	ionic
Kn	Knudsen
sp	support

transport equations. The continuum micro model for electrode statistical property description has been involved. The geometry of this SOFC unit is shown in Fig. 1.

The geometry of the calculation domain is based on the typical planar SOFC design with length 100 mm, air and fuel channel height (rib thickness) 1 mm, interconnect thickness 2.5 mm (1.5 mm without rib part). The simplification of the two-dimensional calculation domain would be reasonable in some of the planar SOFC design where the rib-channel width ratio or channel height–width is relatively small.

The main assumptions made in this model are shown as the following:

(1) The electrochemical reactions spatially occurred along electrode thickness within electrode. The reaction active sites are assumed to be uniformly distributed in each electrode layer. The two conducting phases (electronic and ionic) are considered to be continuous and homogeneous in each layer.
(2) The ionic and electronic charge transport processes take place in PEN (Positive electrode-Electrolyte-Negative electrode assembly) and interconnect. The electronic transport in interconnect as well as the contact and additional resistance due to interconnect were not considered.
(3) H_2–H_2O–N_2 mixtures and air were chosen as the fuel and oxidant of SOFC individually. All gas mixtures are considered as ideal gases.
(4) Convection flux is neglected in the porous electrode compared to diffusion. Pressure gradients in the porous electrode are also neglected.
(5) The outer boundaries of the unit cell, for example, the surface of inter-connector, the inlet and outlet of fuel and air, etc., were considered as thermal insulated.

2.2. Governing equations

The continuum micro-scale PEN sub-model coupled the processes of ion/electronic charge transport, porous electrode diffusion as well as the effects of electrode micro-structures. And in the channel there are only mass conservation equation and energy conservation equation.

2.2.1. Charge conservation

It should be noted that ions only exist in the PEN, and electrons exist in the anode, cathode and inter-connectors. Governing equations for transient charge balance were shown as follows [7,8]:

• Ionic charge balance at the cathode:

$$\frac{C_{dl,ca}S_{act,ca}\partial(V_{ion,ca}-V_{el,ca})}{\partial t}+\nabla\cdot(-\sigma^{eff}_{ion,ca}\nabla V_{ion,ca})=Q_{ion,ca}$$
$$=-i_{0,ca}S_{act,ca}\left(\frac{c^{TPB}_{O_2}}{c^{bulk}_{O_2}}\exp\left(\frac{\alpha n_e F(V_{el,ca}-V_{ion,ca}-V_{ref,ca})}{RT}\right)\right.$$
$$\left.-\exp\left(-\frac{(1-\alpha)n_e F(V_{el,ca}-V_{ion,ca}-V_{ref,ca})}{RT}\right)\right) \quad (1)$$

• Electronic charge balance at the cathode:

$$\frac{C_{dl,ca}S_{act,ca}\partial(V_{el,ca}-V_{ion,ca})}{\partial t}$$
$$+\nabla\cdot(-\sigma^{eff}_{el,ca}\nabla V_{el,ca})=Q_{el,ca}=-Q_{ion,ca} \quad (2)$$

• Ionic charge balance at the anode:

$$\frac{C_{dl,an}S_{act,an}\partial(V_{ion,an}-V_{el,an})}{\partial t}+\nabla\cdot(-\sigma^{eff}_{ion,an}\nabla V_{ion,an})$$
$$=Q_{ion,an}=i_{0,an}S_{act,an}$$

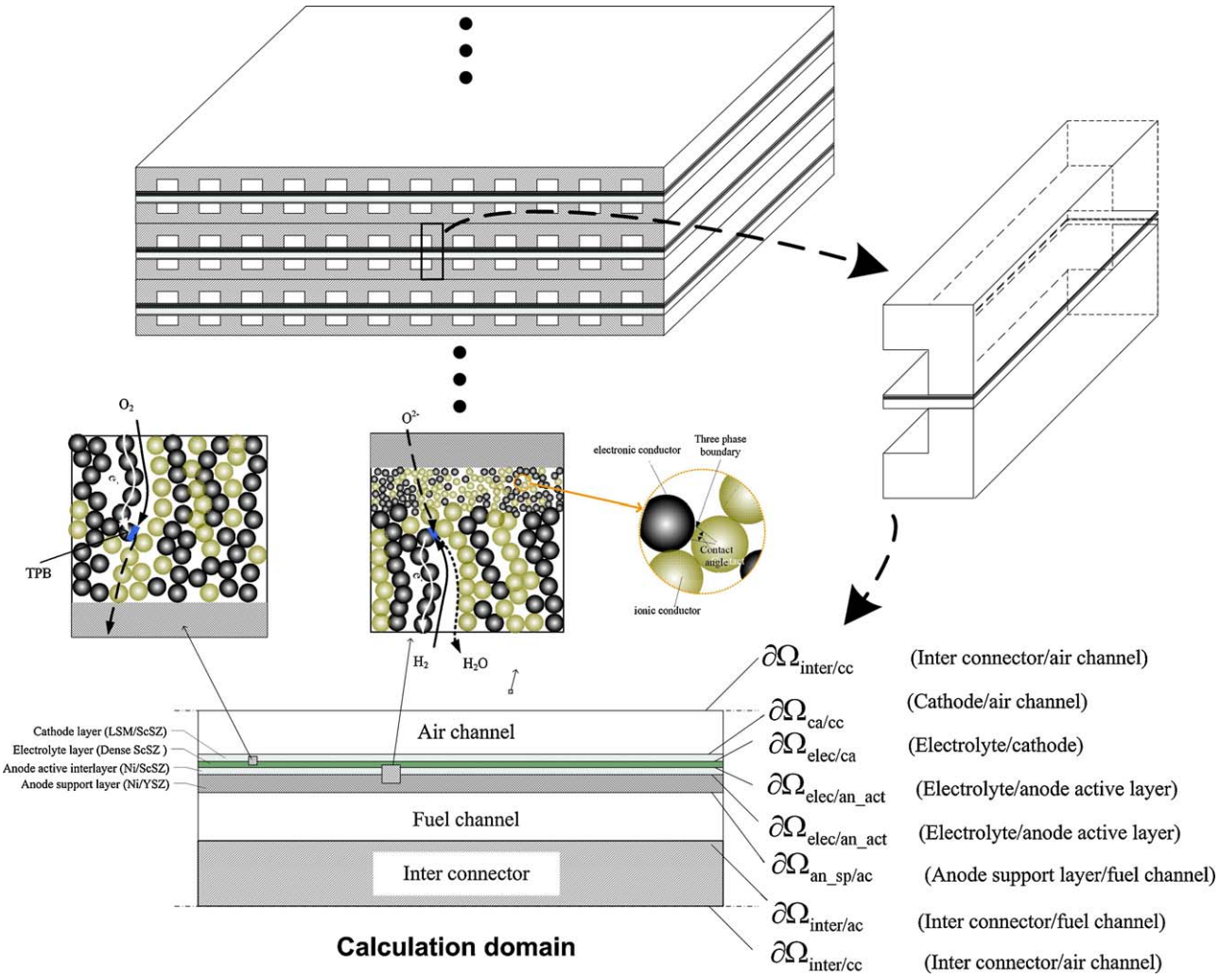

Fig. 1. SOFC unit cell geometry and calculation domain.

$$\times \left(\frac{c_{H_2}^{TPB}}{c_{H_2}^{bulk}} \exp\left(\frac{\alpha n_e F(V_{el,an} - V_{ion,an} - V_{ref,an})}{RT} \right) - \frac{c_{H_2O}^{TPB}}{c_{H_2O}^{bulk}} \times \exp\left(-\frac{(1-\alpha) n_e F(V_{el,an} - V_{ion,an} - V_{ref,an})}{RT} \right) \right) \quad (3)$$

- Electronic charge balance at the anode:

$$\frac{C_{dl,an} S_{act,an} \partial(V_{el,an} - V_{ion,an})}{\partial t} + \nabla \cdot (-\sigma_{el,an} \nabla V_{el,an}) = Q_{el,an} = -Q_{ion,an} \quad (4)$$

where t is time, C_{dl} is the specific interface double-layer capacitance between electronic and ionic conductor phases; Q is the transfer current source; V_{el} and V_{ion} denote the electric potential of the two conductor phases [9].

2.2.2. Mass conservation

The dusty-gas model is used for describing diffusion processes within porous electrode. The dusty-gas model could be formulated as follows while neglecting the pressure gradient in the porous electrode and the implicit relationship between the species mole fraction and molar diffusion fluxes was provided,

$$-c\nabla x_i = \sum_{j=1, i\neq j}^{n} \left(\frac{x_j N_i - x_i N_j}{D_{ij}^{eff}} \right) + \frac{N_i}{D_{kn,i}^{eff}}, \; i = 1, 2, 3, \ldots, n \quad (5)$$

where D_{ij}^{eff} is the effective molecular diffusion coefficients and $D_{kn,i}^{eff}$ is the effective Knudsen diffusion coefficients. This formula can be written as the explicit relationship between species model fractions and molar fluxes using matrix notation,

$$(N_i) = -c[B]^{-1}(\nabla x_i) = -c[\tilde{D}](\nabla x_i) = \left(-c \sum_{j=1}^{n} \tilde{D}_{ij} \nabla x_j \right) \quad (6)$$

where the elements of square matrix $[B]$ can be formulated as,

$$B_{ij} = \begin{cases} \dfrac{1}{D_i^{Kn,eff}} + \displaystyle\sum_{k=1}^{n} \frac{x_k}{D_{ik}^{MS,eff}}, & j = i \\ -\dfrac{x_i}{D_{ij}^{MS,eff}}, & j \neq i \end{cases} \qquad i, j = 1, 2, 3, \ldots, n \quad (7)$$

The $[\tilde{D}]$ is the inverse of the matrix $[B]$, the elements of $[\tilde{D}]$ can be treated as the effective multi component diffusivity according to the dimension of its unit.

Table 1
Governing equations for mass conservation.

Domain	Governing equations
Anode	$\frac{\partial(\varepsilon_{an}\rho_{an}w_{H_2})}{\partial t}+\nabla\cdot\left(-\rho_{an}w_{H_2}\sum_{j=1}^{n}(\tilde{D}_{H_2,j}\nabla x_j)+\rho_{an}w_{H_2}u\right)=\frac{-i_{trans,an}S_{act,an}M_{H_2}}{2F}$
	$\frac{\partial(\varepsilon_{an}\rho_{an}w_{H_2O})}{\partial t}+\nabla\cdot\left(-\rho_{an}w_{H_2O}\sum_{j=1}^{n}(\tilde{D}_{H_2O,j}\nabla x_j)+\rho_{an}w_{H_2O}u\right)=\frac{-i_{trans,an}S_{act,an}M_{H_2O}}{2F}$
Cathode	$\frac{\partial(\varepsilon_{ca}\rho_{ca}w_{O_2})}{\partial t}+\nabla\cdot\left(-\rho_{ca}w_{O_2}\sum_{j=1}^{n}(\tilde{D}_{O_2,j}\nabla x_{O_2})+\rho_{ca}w_{O_2}u\right)=\frac{i_{trans,ca}S_{act,ca}M_{O_2}}{4F}$
Fuel channel	$\frac{\partial(\rho_{an}w_{H_2})}{\partial t}+\nabla\cdot\left(-\rho_{an}w_{H_2}\sum_{j=1}^{n}(\tilde{D}_{H_2,j,chanel}\nabla x_j)+\rho_{an}w_{H_2}u\right)=0$
	$\frac{\partial(\rho_{an}w_{H_2O})}{\partial t}+\nabla\cdot\left(-\rho_{an}w_{H_2O}\sum_{j=1}^{n}(\tilde{D}_{H_2O,j,channel}\nabla x_j)+\rho_{an}w_{H_2O}u\right)=0$
Air channel	$\frac{\partial(\rho_{ca}w_{O_2})}{\partial t}+\nabla\cdot\left(-\rho_{ca}w_{O_2}\sum_{j=1}^{n}(\tilde{D}_{O_2,j,channel}\nabla x_{O_2})+\rho_{ca}w_{O_2}u\right)=0$

Then, we can get,

$$\frac{\partial(\varepsilon\rho w_i)}{\partial t}+\nabla\cdot\left(-\rho w_i\sum_{j=1}^{n}\tilde{D}_{ij}\nabla x_j+\rho w_i u\right)=R_i \tag{8}$$

The equations for electrode mass balances can be summarized as in Table 1.

2.2.3. Momentum conservation

The general formulated non-isothermal weakly compressible Navier–Stokes equation with continuity equation was used to describe the momentum balance in the gas channels,

$$\rho\frac{\partial u}{\partial t}+\rho u\cdot\nabla u=-\nabla p+\nabla\cdot\left[\eta(\nabla u+(\nabla u)^T)-\frac{2}{3}\eta\nabla\cdot u\right],$$
$$\frac{\partial\rho}{\partial t}+\nabla\cdot(\rho u)=0 \tag{9}$$

where u is the velocity vector, p is pressure, η is the dynamic viscosity. ρ is the density. When temperature variation was considered, the density will be a function of the temperature, the momentum equations, continuity equation and temperature equation form a closely coupled system of equations.

In porous sub-domains, the flow variables and fluid properties are defined at any point inside the medium by means of averaging of the actual variables and properties over a certain volume surrounding the point. The flow velocities are defined as superficial volume averages, and they correspond to a unit volume of the medium including both pores and matrix. They are sometimes called Darcy velocities, defined as volume flow rates per unit cross section of the medium. The presented approach eliminates the need for explicit consideration of interfaces. Thus, the flow can be modeled by using the same unknown variables for the entire domain including free flow sub-domains and porous sub-domains. The distinction is made via switching on and off certain terms in the governing equations. The conservation equations are summarized in Table 2.

Table 2
Governing equations for momentum conservation.

Domain	Governing equations
Anode	$\rho\frac{\partial u}{\partial t}+\nabla\cdot(\varepsilon\rho\vec{v}\vec{v})=-\varepsilon\nabla p+\nabla\cdot[\varepsilon\mu_{mix}(\nabla\vec{v}+(\nabla\vec{v})^T)]-\frac{\mu_{mix}}{\alpha}\varepsilon^2\vec{v}$
Cathode	$\rho\frac{\partial u}{\partial t}+\nabla\cdot(\varepsilon\rho\vec{v}\vec{v})=-\varepsilon\nabla p+\nabla\cdot[\varepsilon\mu_{mix}(\nabla\vec{v}+(\nabla\vec{v})^T)]-\frac{\mu_{mix}}{\alpha}\varepsilon^2\vec{v}$
Fuel channel	$\rho\frac{\partial u}{\partial t}+\nabla\cdot(\rho\vec{v}\vec{v})=-\nabla p+\nabla\cdot[\mu_{mix}(\nabla\vec{v}+(\nabla\vec{v})^T)]$
Air channel	$\rho\frac{\partial u}{\partial t}+\nabla\cdot(\rho\vec{v}\vec{v})=-\nabla p+\nabla\cdot[\mu_{mix}(\nabla\vec{v}+(\nabla\vec{v})^T)]$

Table 3
Governing equations for energy balance.

Domain	Governing equations
Solid structures	$\frac{\partial(\rho C_p T)}{\partial t}+\nabla\cdot(-\lambda_{eff}\nabla T)=Q_{heat}$
Fuel and air channels	$\frac{\partial(\rho C_p T)}{\partial t}+\nabla\cdot(-\lambda\nabla T+\rho C_p T u)=0$

2.2.4. Energy balance

The heat transport processes within SOFC unit cell are usually complex as shown in following:

- MEA: conductive and radiative heat transfer, and the heat sources include the ohmic heat due to ionic and electronic conducting, the reversible heat effects of entropy change in electrochemical reactions, as well as the irreversible heat generation due to activation polarizations.
- Interconnect: conductive and radiative heat transfer.
- Gas channels: convective heat transfer.

The governing equations for energy balance are shown in Table 3.

λ_s and λ_g are thermal conductivities of solid phase and gas phase materials in porous electrodes. Q_{heat} is the heat source term, and can be calculated as following equation in different solid structures,

$$Q_{heat}=\begin{cases}0,\text{ inter-connector}\\ Q_{ohm},\text{ electrolyte}\\ Q_{ohm}+Q_{rev}+Q_{irr},\text{ porous electrode}\end{cases} \tag{10}$$

where the Q_{ohm} is the ohmic heat and can be calculated as,

$$Q_{ohm}=\begin{cases}\frac{i_{ion}^2}{\sigma_{ion}},\text{ electrolyte}\\ \frac{i_{ion}^2}{\sigma_{ion}}+\frac{i_{el}^2}{\sigma_{el}},\text{ porous electrode}\end{cases} \tag{11}$$

where i is local electronic or ionic current density, σ is electric conductivity.

Q_{rev} is the reversible heat effects of entropy change in electrochemical reactions, and can be calculated as,

$$Q_{rev}=\begin{cases}\frac{i_{trans,an}S_{act,an}T(S_{H_2O}+2S_{e^-}-S_{H_2}-S_{O^{2-}})}{2F},\text{ anode}\\ \frac{i_{trans,ca}S_{act,ca}T(S_{O^{2-}}-(1/2)S_{O_2}-2S_{e^-})}{2F},\text{ cathode}\end{cases} \tag{12}$$

where S is the molar entropies of species. Then the anode entropy change can be calculated by subtracting cathode entropy change from whole the entropy change of electrochemical reaction. Q_{irr} is the irreversible heat generation due to activation polarizations which can be formulated as,

$$Q_{irr}=|\eta Q_{el}|=|\eta Q_{ion}| \tag{13}$$

For the gas channels, the energy balance equations can be formulated by considering convective and conductive heat transfer processes,

$$\frac{\partial(\rho C_p T)}{\partial t} + \nabla \cdot (-\lambda \nabla T + \rho C_p T u) = 0 \quad (14)$$

where C_p is the specific heat capacity, and λ is thermal conductivities of gas in gas channels.

The radiative heat transfer between the MEA solid structure and interconnect has been considered by introducing a heat flux of surface-to-surface radiation in heat flux boundary conditions at electrode/channel and interconnect/channel interfaces.

$$q_{\text{rad,electrode-inter}} = \frac{\sigma_B(T^4_{\text{electrode}} - T^4_{\text{inter}})}{((1/\varepsilon_{\text{electrode}}) - 1) + (1/F_{\text{electrode-inter}}) + (A_{\text{electrode}}/A_{\text{inter}})((1/\varepsilon_{\text{inter}}) - 1)} \quad (15)$$

$$q_{\text{rad,inter-electrode}} = \frac{\sigma_B(T^4_{\text{inter}} - T^4_{\text{electrode}})}{((1/\varepsilon_{\text{inter}}) - 1) + (1/F_{\text{inter-electrode}}) + (A_{\text{inter}}/A_{\text{electrode}})((1/\varepsilon_{\text{electrode}}) - 1)} \quad (16)$$

where ε is surface emissivity. σ_B is the Stefan–Boltzmann constant ($5.67e{-}8\,W\,m^{-2}\,K^{-4}$) F is the radiative view factor which can be calculated according to the SOFC geometry.

2.3. Boundary conditions

In order to solve the system of coupled partial differential equations for charge, mass, momentum and energy balances, the name of boundary conditions are specified in Fig. 1. First of all, the up and bottom boundaries $\partial\Omega_{\text{inter/cc}}$ were set as periodical for each physical field. The detailed settings of other boundaries were listed as following:

Ionic charge balance. At the electrode/electrolyte interfaces $\partial\Omega_{\text{ca/elec}}$, $\partial\Omega_{\text{an\_act/elec}}$, the continuity boundary condition was applied to specify that the normal ionic current are continuous across the interior boundary. The electric-insulation condition, specifies no current flow across the boundary, was applied at other boundaries.

Electronic charge balance. At the electrode/channel interfaces $\partial\Omega_{\text{an\_sp/ac}}$, $\partial\Omega_{\text{ca/cc}}$, the electric potentials $V_{\text{cell,an}}$ and $V_{\text{cell,ca}}$ were specified, respectively. Here, $V_{\text{cell,an}}$ was set as zero and $V_{\text{cell,ca}}$ is set as the cell working voltage. At the electrode/electrolyte interfaces $\partial\Omega_{\text{ca/cc}}$, $\partial\Omega_{\text{an\_act/ac}}$ and other boundaries, electric-insulation conditions were specified.

Mass balance. The mass fraction was specified at the inlet of fuel and air channels while the convective flux boundary condition, which indicates that the mass transport out of the domain is dominated by convection, was specified at outlets of gas channels. At the electrode/electrolyte interfaces $\partial\Omega_{\text{ca/elec}}$, $\partial\Omega_{\text{an\_act/elec}}$ and other boundaries, the gas insulation conditions were specified.

Momentum balance. The velocity was specified at the inlets of fuel and air channels while the pressure condition was specified at the outlets of the channels. Other boundaries were set as walls with no slip which indicates that the velocity of the gas at the wall is zero.

Energy balance. The gas temperature was given at the inlet of fuel and air channels. The convective heat flux boundary, which means $n \cdot (-\lambda \nabla T) = 0$, was specified at the outlets of gas channels. Energy transport processes of gas and solid are coupled at the electrode/channel interfaces and interconnect/channel interfaces by specifying that the temperature are continuous across the boundaries, and the radiation heat flux boundary was also specified at these interfaces. The other boundaries were specified as heat insulation.

2.4. Model solution and EIS spectra synthesis

The problem was solved for a given cell voltage. The perturbation voltage is chosen as 10 mV to assure the EIS linearity, and in fact this value is set as the same with that for EIS experimental tests. The outputs of the model are the distributions of current density and species concentrations. The calculations were performed using the finite element commercial software COMSOL MULTIPHSICS®. Since large differences exist in length scales of MEA structure and channels/interconnect, the asymmetry mapping structured quadrilateral mesh was used in the solution. The mesh consists of 4940 elements with the number of freedom degree 20,036 which could make sure the calculation resolution independent with the mesh element number. We have placed 76 elements along axial direction and 65 elements along electrode thickness direction. For electrode thickness direction, we use 5 elements in electrolyte, cathode and anode active layer, and use 12 elements in anode channel, cathode channel. For anode support layer and current collector layer, 13 elements were used. The default stationary nonlinear solver (uses damped Newton method with direct linear system solver UMFPACK) of COMSOL MULTIPHSICS® was used for a certain operating case, while the parametric nonlinear solver was used to get the EIS spectra. The relative tolerance of the model was specified as 1e−5.

The average current density was calculated as following equation in electrolyte layer with constant coordinate y:

$$i_{\text{avg}} = \frac{1}{L}\int_0^L i_{\text{ion,local}}\,dx \quad (17)$$

where $i_{\text{ion,local}}$ is the local ionic current density in electrolyte layer and L is the length of the calculation domain along x direction.

In order to generate a complete EIS spectrum, the model needs to be run for several periods just like the experimental measurements of the EIS. The time step is equal to one twentieths periods, and the time span is equal to 15 periods. The detailed calculation method can be found in our previous studies [10]. While, the two-dimensional EIS simulation is a time-consuming problem. We calculate the current response at different frequencies separately using four small computation workstation (Intel Xeon 3.2 GHz, 8GB Memory). The total calculation time for a whole EIS spectrum is around 2 h. In order to calculate the impedance of the fuel cell, the model is simulated at the selected voltage for 10 s to achieve steady state. Then, the model initial condition was set as the steady state, and the model is solved repeatedly with sinusoidal signals superimposed on the voltage.

3. Results and discussion

3.1. Model parameters

From the model development section of charge balance and mass balance equations, the effective reaction area, TPB area and TPB length are needed in the calculation. The parameter S_{TPB} can be formulated by using the particle coordination number in binary

random packing of spheres together with percolation theory as [11,12]

$$S_{TPB} = \frac{\pi \sin^2 \theta r_{el}^2 N_{tot} n_{el} n_{io} Z_{el} Z_{io} P_{el} P_{io}}{Z} \quad (18)$$

where Z is the mean coordination number, r_{el} is the mean radius of the electronic conductor particle, θ is the contact angle between the electronic and ionic conductors particles, N_{tot} is the total number of particles per unit volume, n_{el} and n_{io} are the fraction number of electronic and ionic conductor particles, Z_{el} and Z_{io} are the coordination numbers of electron and ion conductor particles, and P_{el} and P_{io} are the whole range connection probabilities of the same kind particles. Here S_{TPB} is treated as the contact area of different types of particles.

Similar to the calculation S_{TPB}, the parameter L_{TPB} (TPB length per unit volume) can be calculated as,

$$L_{TPB} = 2\pi r_{el} \sin\theta N_{tot} n_{el} Z_{el\text{-}io} P_{el} P_{io} \quad (19)$$

The pore structure of the anode support layer was characterized using mercury porosimeter. The mean pore diameter, porosity and total pore area were found to be 0.387 μm, 0.335 and $8.54 \times 10^6\ m^2\ m^{-3}$, respectively. To simplify the calculation, the mean particle diameters of the two conductors are assumed to be the same and equal to the mean pore diameter [13]. With this assumption and the expressions of effective reaction areas, the calculated value of S_{TPB} in the anode support layer is 2.22×10^5. The mean pore size in anode support layer is assumed 1.2 and 1.5 times of that in cathode layer and anode active layer based on SEM image from quantitative stereology.

The physical properties of gas mixture, e.g. specific heat capacity, heat conductivity, viscosity, et al. were calculated in the well-correlated equations with temperature in the works of Young et al. [14]. The physical properties of solid structures are listed in Table 4. These parameter values were based on the values from published literatures and the temperature dependence of the heat conductivity, density and heat capacity of all solid materials were all considered negligible in the temperature range concerned here.

3.2. PEN sub model validation

The button cell experimental data was used to validate the PEN sub-model by neglecting the effect of momentum and heat transfer. The test setup, validation results can be found in our previous paper [7–10]. The parameters, include charge transfer reaction kinetic parameter, tortuosity and interface capacity for both cathode and anode were well validated using experimental polarization curves obtained on a SOFC button cell and a symmetric cathode cell, whose material and structure are exactly kept the same with the MEA in the unit cell in this paper. The experimental data used in the model validation include the I–V curves and EIS spectra at following operating conditions:

- Different cell temperatures at 750 °C, 800 °C and 850 °C with oxygen or air oxidant
- N_2 dilution at 800 °C and 850 °C with N_2 content in the dry fuel mixture: 0, 20%, 40%, 60% and 80%.

Fig. 2 shows the comparison results between simulated and experimental polarization curves and EIS spectra. It can be seen that the PEN EIS model can well predict the experimental data at different temperatures and with different fuel compositions. These validations will be the basis of the unit cell two-dimensional EIS model.

Table 4
Model parameters.

Parameters	Value
Electric conductivity ($S\ m^{-1}$)	
Ionic conductor ScSZ, σ_{ScSZ}	$6.92e4 \exp(-9681/T)$
Ionic conductor YSZ, σ_{YSZ}	$3.34e4 \exp(-10{,}300/T)$
Electronic conductor LSM, σ_{LSM}	$4.2e7/T \exp(-1150/T)$
Electronic conductor Ni, σ_{Ni}	$3.27e6-1065.3T$
Equivalent ionic conductivity of electrolyte layer	$0.002T-1.4483$
Heat conductivity ($W\ m^{-1}\ K^{-1}$)	
Anode (support/active layers) λ_{an_sp}, λ_{an_act}	6.23
Cathode, λ_{ca}	9.6
Electrolyte, λ_{elec}	2.7
Interconnect, λ_{inter}	25
Density ($kg\ m^{-3}$)	
Anode (support/active layers), ρ_{an_sp}, ρ_{an_act}	6870
Cathode, ρ_{ca}	6570
Electrolyte, ρ_{elec}	2000
Interconnect, ρ_{inter}	8000
Heat capacity ($J\ kg^{-1}\ K^{-1}$)	
Anode (support/active layers), C_{p,an_sp}, C_{p,an_act}	420
Cathode, $C_{p,ca}$	390
Electrolyte, $C_{p,elec}$	300
Interconnect, $C_{p,inter}$	500
Emissivity	
Anode	0.8
Cathode	0.8
Interconnect	0.1
Parameters of electrochemical reaction kinetics	
Interface conductivity $\beta_{an\_sp}/\beta_{an\_act}/\beta_{ca}$ ($\Omega^{-1}\ m^{-2}$)	6.8e12/6.8e12/5.8e10
Activation energy $E_{act,an\_sp}/E_{act,an\_act}/E_{act,ca}$ ($J\ mol^{-1}$)	120,000/120,000/130,000
Microstructures	
Anode support layer porosity/tortuosity/pore radius (μm)	0.364/16.5/0.48
Anode active layer porosity/tortuosity/pore radius (μm)	0.364/16.5/0.31
Cathode porosity/tortuosity/pore radius (μm)	0.364/3/0.4

3.3. Two dimensional EIS spectra modeling at constant temperature

3.3.1. Effects of operating voltage on 2D EIS spectra

For the convenience of comparison between cases with different working status, one set of operating conditions of cell referred to "base case" was selected as shown in Table 5,

Fig. 3 shows the calculated parameter distributions of SOFC unit cell cross section at 0.7 V and at constant temperature 800 °C in the base case. It can be seen in Fig. 3(a) that the ionic current density decreases along flow channel direction. The current density value at the position of fuel inlet is around $5000\ A\ m^{-2}$ which is near the corresponding button cell performance as shown in Fig. 2, and the local current density gradually decreases to around $1000\ A\ m^{-2}$ at the anode outlet. As shown in Fig. 3(b) the H_2 molar fraction decrease fast along flow channel due to the continuous H_2 electrochemical consumption, and thus the local cell reversible voltage decease and the local activation and concentration polarization losses increase.

Table 5
Model parameters at base case.

Operating conditions	Anode	Cathode
Gas inlet mole fraction	96% H_2, 4% H_2O	21% O_2, 79%N_2
Gas inlet mole flowrate ($mol\ h^{-1}$)	0.0225	0.58
Gas inlet velocity ($m\ s^{-1}$)	0.008	0.208
Gas outlet pressure (Pa)	101,325	101,325
Flow configuration	Counter flow	
Cell voltage	0.7	

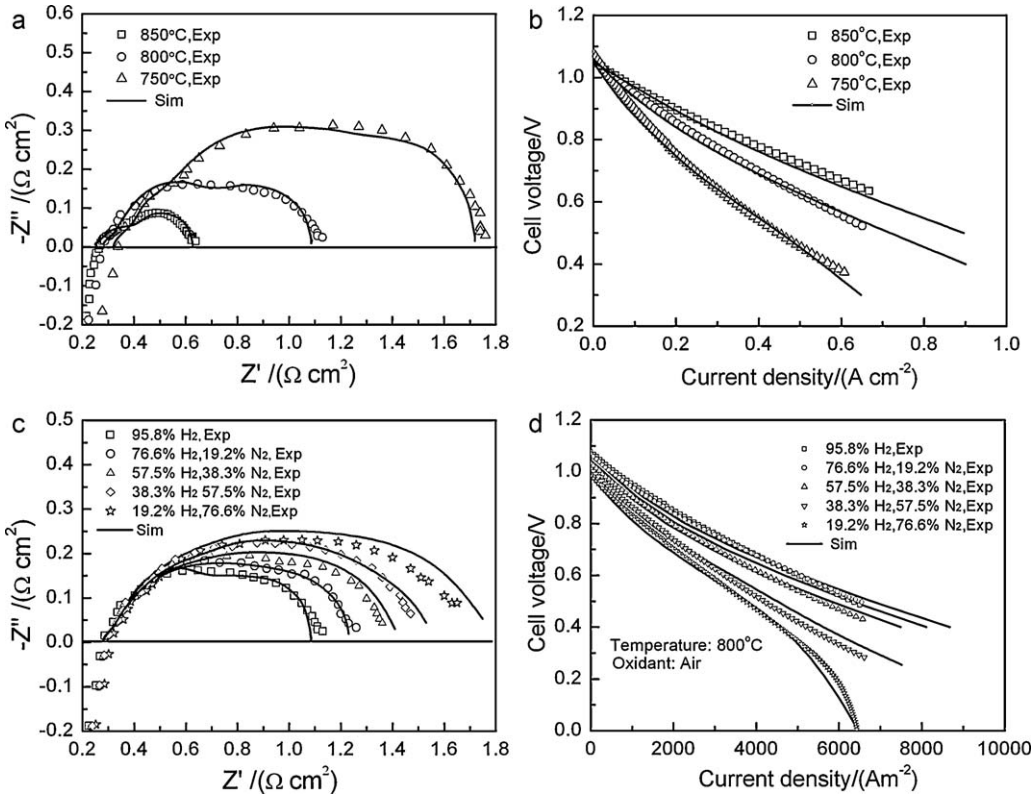

Fig. 2. Experimental and simulated results comparison: (a) EIS spectra at 750/800/850 °C; (b) polarization curves at 750/800/850 °C; (c) EIS spectra with different fuel compositions; (d) polarization curves with different fuel compositions.

Since the air flow rate is far larger than the fuel flow rate, the O_2 molar fraction varies slightly.

Fig. 4 shows the calculated local impedance spectra in the base case at different operating cell voltages at constant temperature 800 °C. *X* indicated dimensionless *x*-axis along fuel flow direction. The impedance increases from anode gas inlet towards anode gas outlet due to the increased charge transfer and mass transfer impedance due to fuel consumption. It can be deduced that the average impedance can predict the two impedance half circles which indicated two types of limiting processes, but it is hard to represent the impedance status at different positions along flow channel. Especially at the downstream of the flow channel, the low frequency impedance half circle increase fast due to the mass transfer in both electrode thickness direction and in flow channel direction affected by the product accumulation. These results indicated that 1D impedance model is not enough for using in unit cell impedance spectra interpretation, 2D effect, e.g. convective-diffusion impedance, has to be considered. Also, it can be seen that the radius of impedance half circle shrinks from 0.9 V to 0.7 V when *X* is larger than 0.75 due to the decrease of activation polarization resistance. At this time, the effect of diffusion limitation is not obvious. While for $X = 1$, the low frequency impedance for cell voltage at 0.7 V increase fast due to the increase of concentration losses at the flow channel down stream.

3.3.2. Effects of fuel flow rate on 2D EIS spectra

Fig. 5 shows the calculated the local impedance spectra at constant temperature 800 °C with cell voltage at 0.7 V by increasing the fuel flow rate for 4 times as in the base case from 0.0225 mol h^{-1} to 0.09 mol h^{-1}. The results indicated that the low frequency impedance half circle is very small at fuel inlet, and increase gradually along flow direction. In this case, the fuel utilization is only kept at 0.22 due to the relatively large fuel flow rate and this means that the fuel is not consumed much. Thus, it can be seen that the low frequency impedance half circle does not have significant increase as shown in the Fig. 4. This suggests that the average impedance can be good prediction in the unit cell impedance only when the fuel and air utilization are small.

3.4. Two dimensional EIS spectra modeling by coupling electro-thermal effects

3.4.1. Electro-thermal impedance effects

When the EIS spectra tests are carried out on the button cell, the operating condition is kept at well constant temperature oven. Thus the current variation in EIS tests is small, and the effects of temperature variation due to the cell current variation can be neglected.

However, if considering a SOFC unit cell or a SOFC stack, the temperature effects from AC current can possibly be significant. Thus, we further investigate the local impedance spectra in different positions along flow channel with consideration of temperature response as shown in Fig. 6. The results indicated that the heat transfer will have significant effects on the impedance spectra especially at low frequency part. From local impedance spectra calculation, the inductive half circle appeared in the low frequency part. The effect of temperature variation is not significant near the fuel inlet. But the effects gradually increase. Before $X = 0.5$, the effects are mainly represented as inductive loops. When at the down stream of fuel channel (e.g. $X > 0.5$), we could see the third impedance half circle in the spectra. The impedance leaded by electro-thermal effects increase to the value compatible to the low frequency impedance half circle (mass transfer impedance).

To further understand the effects of temperature variation on EIS spectra, the qualitative analysis of impedance characteristics can be done when considering state variables include the operating voltage *V*, reacting gas concentration *C* and temperature *T*. In fact,

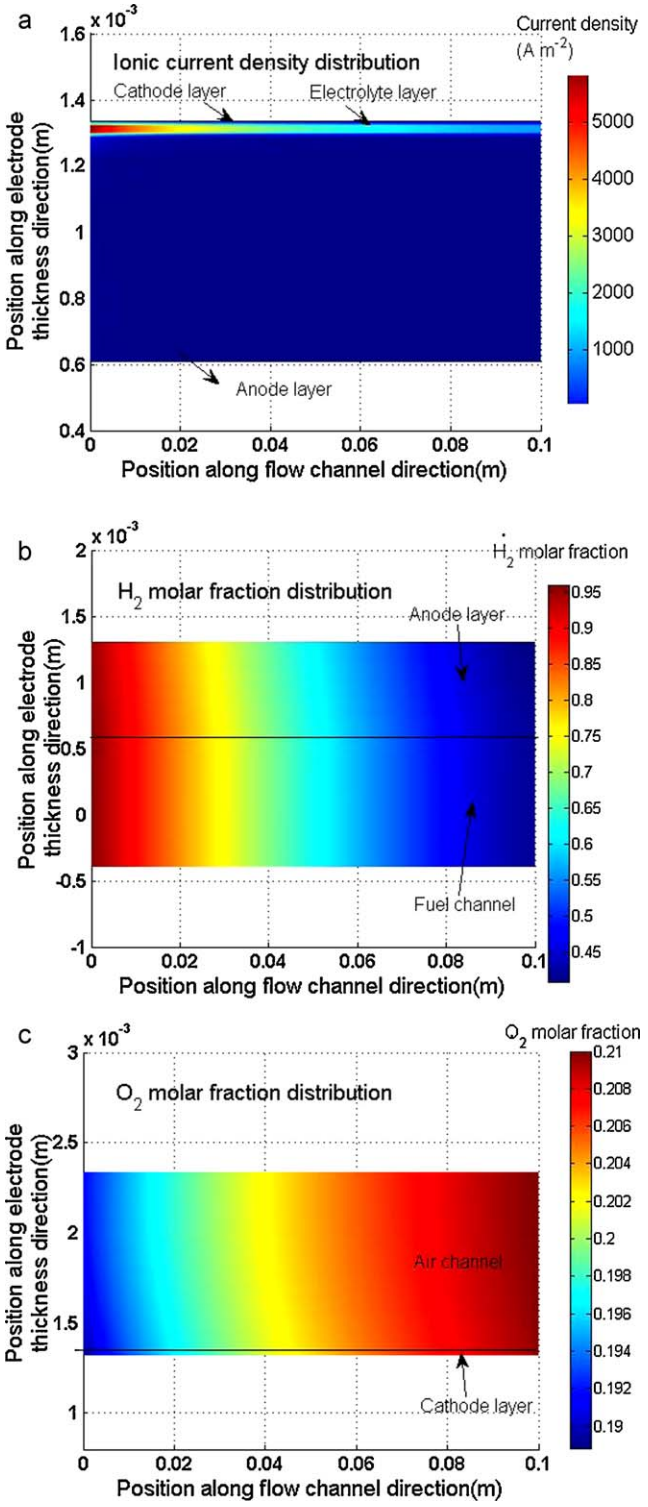

Fig. 3. Calculated parameter distributions: (a) ionic current density; (b) H_2 molar fraction; (c) O_2 molar fraction at 0.7 V and at constant temperature 800 °C in the base case.

when at constant operating pressure, by assuming at the steady sate, the Faraday current I_F can be written as [15]:

$$I_F = f(V, T, C_i) \quad i = 1, 2, 3, \ldots \tag{20}$$

When the EIS spectra is located near the fuel inlet (e.g. non-dimensional position $Z = 0$ along flow channel direction). Since the fuel concentration is high at fuel inlet, in order to simplify

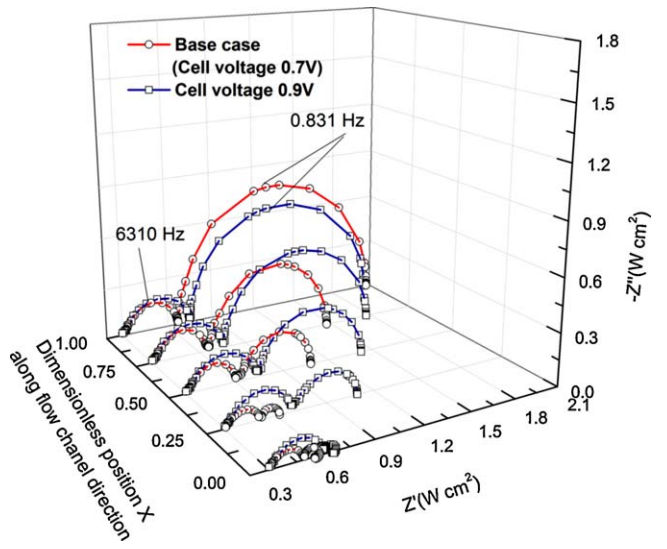

Fig. 4. Calculated local impedance spectra at 0.7 V and 0.9 V and at constant temperature 800 °C (1 mHz to 1 MHz).

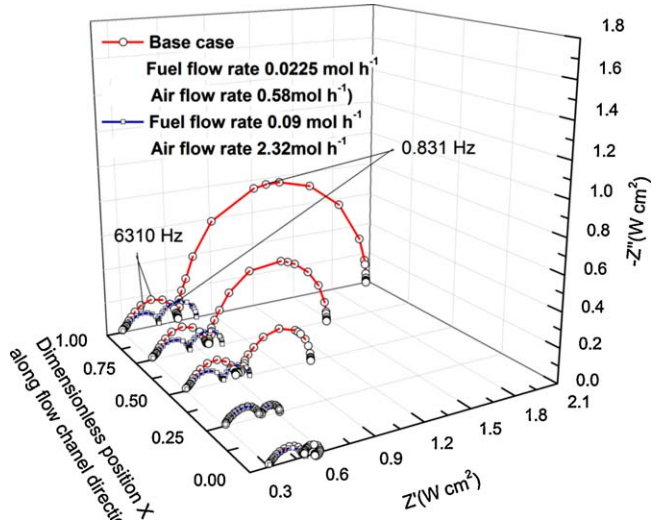

Fig. 5. Calculated local impedance spectra at 0.7 V with increasing fuel flow rate at constant temperature 800 °C (1 mHz to 1 MHz).

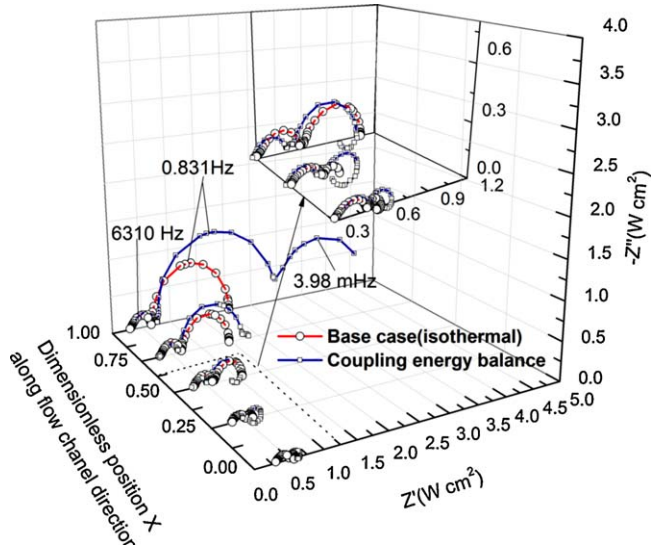

Fig. 6. Calculated global and local impedance spectra in the base case at 0.7 V considered energy balance (1 mHz to 1 MHz).

the discussions, the state variables reacting gas concentration C could be assumed to be constants. Thus, the Faraday current is considered to the function of state variables V and T. Then, in order to get the expression of Faraday admittance Y_F, the I_F can be Taylor expanded to linear order as:

$$\Delta I_F = \left(\frac{\partial I_F}{\partial V}\right)_T \Delta V + \left(\frac{\partial I_F}{\partial T}\right)_V \Delta T \tag{21}$$

Next, to express ΔI_F as the only function of ΔV, the ΔT needs to be expressed as the function of ΔV,

$$\Delta\left(\frac{\partial T}{\partial t}\right) = j\omega\Delta T = \left(\frac{\partial}{\partial V}\left(\frac{\partial T}{\partial t}\right)\right)_T \Delta V + \left(\frac{\partial}{\partial T}\left(\frac{\partial T}{\partial t}\right)\right)_V \Delta T \tag{22}$$

$$\frac{\Delta T}{\Delta V} = \frac{((\partial/\partial V)(\partial T/\partial t))_V}{j\omega - ((\partial/\partial T)(\partial T/\partial t))_V} \tag{23}$$

Then, the faradic admittance Y_F can be obtained as,

$$Y_F = \frac{\Delta I_F}{\Delta V} = \left(\frac{\partial I_F}{\partial V}\right)_T + \left(\frac{\partial I_F}{\partial T}\right)_V \frac{\Delta T}{\Delta V} = \frac{1}{R_t} + \frac{B}{j\omega + A} \tag{24}$$

where the parameters A, B and R_t are formulated as:

$$A = -\left(\frac{\partial}{\partial T}\left(\frac{\partial T}{\partial t}\right)\right)_V \tag{25}$$

$$B = m \cdot b = \left(\frac{\partial I_F}{\partial T}\right)_V \left(\frac{\partial}{\partial V}\left(\frac{\partial T}{\partial t}\right)\right)_T \tag{26}$$

$$R_t = \left(\frac{\partial V}{\partial I_F}\right)_T \tag{27}$$

To satisfy the stability constraint of the electrochemical system, the value of $(\partial/\partial T)(\partial T/\partial t)_V$ should be negative, which means the parameter A should be positive. R_t is also a positive parameter since the V is always increase with I_F at certain temperature, and this represent the process within electric double layer. And, the sign of B will depend on the values of m and b.

It is easy to judge that the value of m, represented as $(\partial I_F/\partial T)_V$, should be positive since the Faraday current increase with the temperature at certain operating voltage. While, it is not easy for the value of b directly. Since the electrochemical system is operated at steady state, thus $(\partial T/\partial t)_T$ should be equal to zero. Then, we have,

$$\frac{dT}{dt} = -\frac{dV}{dt}\left(\frac{\partial T}{\partial V}\right)_T \tag{28}$$

Then, this formula can be transformed as:

$$\frac{dT}{dV} = -\frac{((\partial/\partial V)(\partial T/\partial t))_T}{((\partial/\partial T)(\partial T/\partial t))_V} = -\frac{b}{A} \tag{29}$$

$$b = A\frac{dT}{dV} \tag{30}$$

When V increases, the current and the temperature increase. Thus, b will have the same sign with A, and is positive in this situation. And, this also indicates that the $B > 0$. Then, the admittance Y_F can be further formulated as:

$$Y_F = \frac{1}{R_t} + \frac{B}{j\omega + A} = \frac{1}{R_t} + \frac{1}{j\omega L + R_o} \tag{31}$$

where $R_o = A/B > 0$, $L = 1/B > 0$. In fact, this admittance is the expression of a equivalent circuit with the parallel connection of a resistor R_t and a complex element with serious connection of R_o and L. The circuit formula should be $(R_t(R_oL))$. Thus, according to above discussion, it is obvious that when considering thermal effects, the inductive loop will be observed in the EIS spectra.

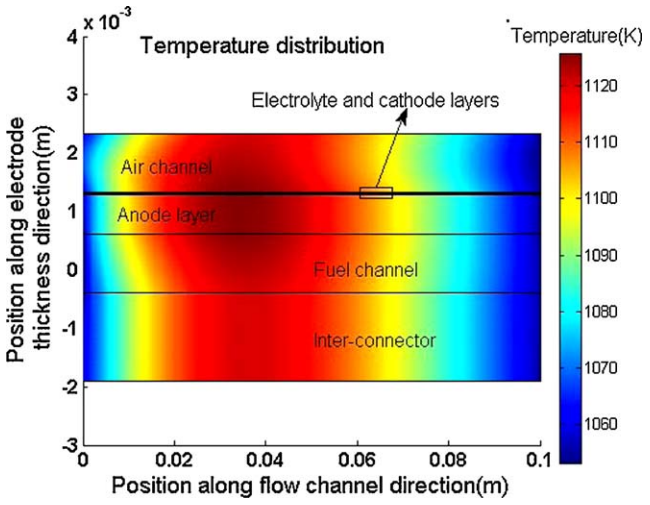

Fig. 7. Calculated temperature distribution considering thermal effects at steady state in the base case.

When considering the local EIS spectra near the fuel outlet, the concentration polarization will became significant and the analytical analysis will be more difficult [15]. While, in order to simplify the analysis, if we consider an extreme condition in which the effects of gas concentration is far significant than that of temperature at the downstream of flow channel, the impedance will totally represent the large low frequency capacitive reactance circle. Thus, we could further deduced that the whether the local EIS spectra is capacitance circle or inductance will depend on the complex coupling interaction among charge transfer reaction, gas transport process, temperature variation. And, in fact, this is one of the important reason to develop a 2D mechanistic EIS model in present manuscript. And, from above preliminary calculation and theoretical discussions, it should be noted that the SOFC unit cell impedance contains the effects which is hard to be interpreted by common zero- or one-dimensional EIS spectra models.

3.4.2. Temperature distribution and response

Fig. 7 shows the calculated temperature distribution considering thermal effects at steady state in the base case. The fuel and oxidant temperature increase along flow channel near fuel inlet, and the maximum temperature is located at around 1/3 flow channel length from fuel inlet. The effects from temperature variation may lead to misinterpretation of the diffusive losses. In this situation, 2D EIS spectra model will be significantly important. In addition, it suggests that researchers should pay more attention in unit cell impedance experimental measurements to avoid the electro-thermal coupling effects, and to clarify the contributions to the impedance from different reaction and transport processes.

Fig. 8 shows the calculated current density and temperature responses in base case operating condition. It can be seen that in this case the temperature is not a constant but shows a periodic-like response like current density. In fact, the temperature and current density response shows the coupling effects from temperature variation and accumulation effects at flow channel downstream. When the $Z = 0$, it can be seen that the temperature response is relatively smooth since only the energy balance is coupled. While, when the $Z = 0.5$ and $Z = 1$, the temperature shows irregular response due to the accumulation effects along the flow channel. However, the response of both temperature and current density are still periodic. This phenomenon suggests that the temperature variation affect the impedance spectra shapes.

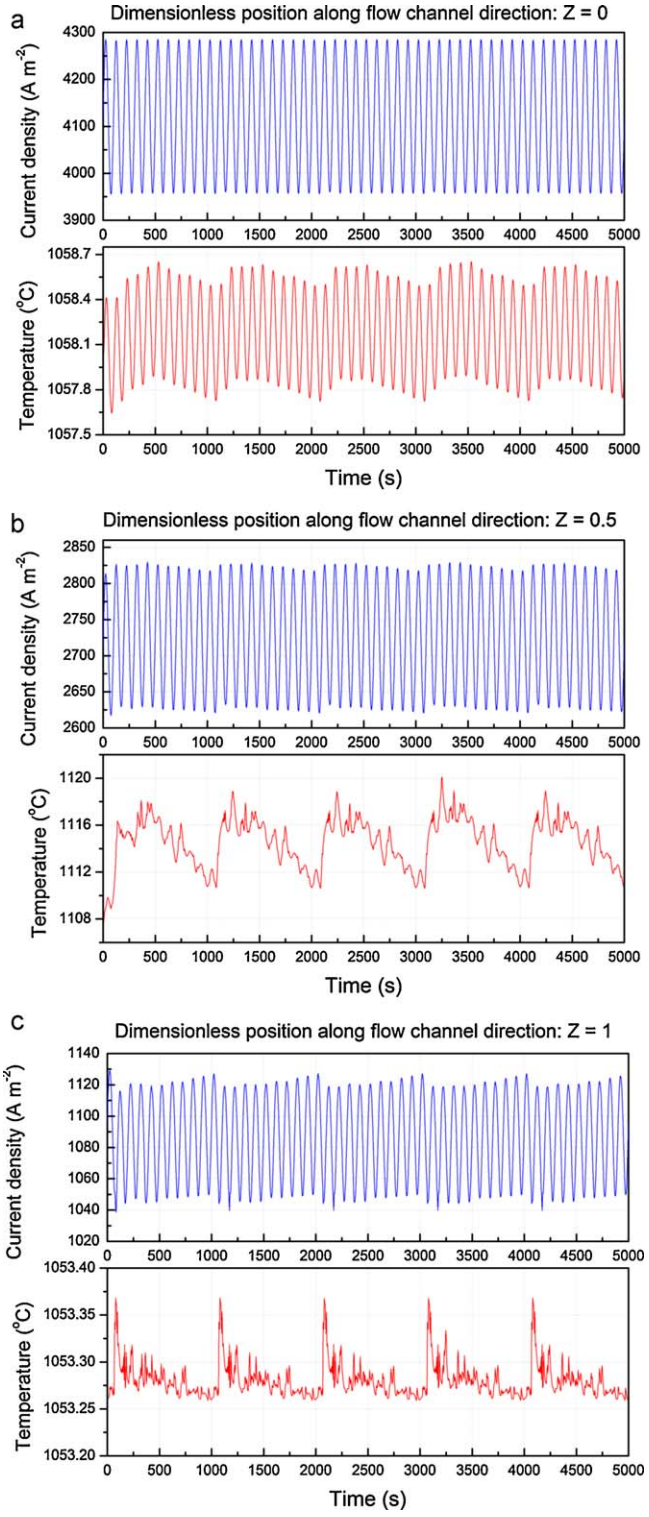

Fig. 8. Calculated current density and temperature response in the base case at different position along flow channel direction: (a) $Z = 0$; (b) $Z = 0.5$ and (c) $Z = 1$.

3.4.3. *Effects of operating voltage on electro-thermal impedance*

Fig. 9 further predicts the effects of operating voltage on electro-thermal impedance. The results indicate that the third impedance half circle due to thermal effects at 0.7 V is larger than that at 0.9 V. In fact, at lower cell voltage, the current density is relatively larger, and thus the thermal effects from polarization heat became significant. Especially at the downstream of the flow channel, the third impedance half circle increase fast due to the coupling temperature

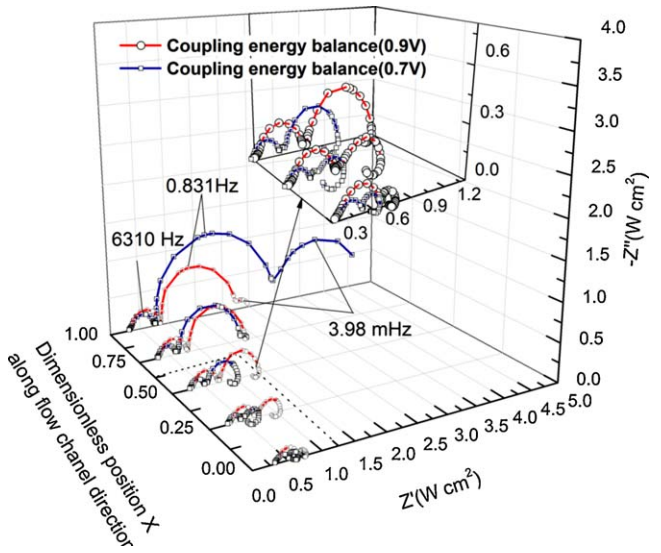

Fig. 9. Effects of operating cell voltage on local electro-thermal impedance spectra (1 mHz to 1 MHz).

variation and mass transfer in both electrode thickness direction and in flow channel direction affected by the product accumulation. These results further indicated that the periodical temperature swing due to the perturbation voltage and current density will lead to unusual electro-thermal impedance effects. While, this effect will became significant at relatively larger current density operation mode, and it is very hard to be interpreted by an circuit element in a equivalent circuit model or 1D impedance model. These further demonstrate the priority of direct electrochemical impedance modeling approach by integrating the effects of multi-dimensional cell geometry and multi-physics coupling.

4. Conclusions

In this paper, a two-dimensional (2D) EIS simulation approach was developed by solving a SOFC unit cell transient model with imposed sinusoidal voltage perturbations at different frequencies. The transient SOFC unit cell model described the intricate interdependency among the ionic conduction, electronic conduction, multi-component species transport, electrochemical reaction processes and electrode microstructure within Membrane-Electrode-Assembly (MEA) as well as the coupling processes of mass, energy, momentum transport and charge transfer within flow channel and inter-connectors. The main conclusions from 2D EIS simulation results include:

The convection-diffusion process along the flow channel has significant effects on the low frequency half circle of the impedance spectra. The global impedance is hard to represent the impedance status at different positions along flow channel.

The temperature oscillations accumulate along the flow channels, and then affect the current response which probably leads to electro-thermal impedance effects.

Equivalent circuit or 1D EIS models are not sufficient to describe the SOFC unit cell impedance response, and the work in this study can be helpful in interpreting EIS spectra, as illustrated in identifying the contribution of different reaction and transport limitations.

Acknowledgement

The supports from Projects 20776078 and 51106085 (National Natural Science Foundation of China, NSFC) is highly appreciated.

References

[1] J. Fleig, J. Maier, J. Electrochem. Soc. 144 (11) (1997) L302.
[2] A. Bieberle, L.J. Gauckler, Solid State Ionics 146 (2002) 23.
[3] W.G. Bessler, Solid State Ionic 176 (2005) 997.
[4] H. Zhu, R.J. Kee, J. Electrochem. Soc. 153 (2006) A1765.
[5] I.A. Schneider, M.H. Bayer, P. Boillat, G.G. Scherer, ECS Trans. 11 (2007) 461.
[6] I.A. Schneider, M.H. Bayer, A. Wokaun, G.G. Scherer, J. Electrochem. Soc. 155 (2008) B704.
[7] Y.X. Shi, N.S. Cai, C. Li, C. Bao, E. Croiset, J.Q. Qian, Q. Hu, S.R. Wang, J. Power Sources 172 (2007) 235.
[8] Y.X. Shi, N.S. Cai, C. Li, C. Bao, E. Croiset, J.Q. Qian, Q. Hu, S.R. Wang, J. Power Sources 172 (2007) 246.
[9] Y. Shi, N. Cai, C. Li, C. Bao, E. Croiset, J.Q. Qian, Q. Hu, S.R. Wang, ECS Trans. 7 (1) (2007) 1889.
[10] Y. Shi, N. Cai, C. Li, C. Bao, E. Croiset, J.Q. Qian, Q. Hu, S.R. Wang, J. Electrochem. Soc. 155 (3) (2008) B270.
[11] P. Costamagna, P. Costa, V. Antonucci, Electrochim. Acta 43 (1998) 375–394.
[12] S.H. Chan, Z.T. Xia, J. Electrochem. Soc. 148 (2001) A388–A394.
[13] J. Divisek, R. Wilkenhoner, Y. Volfkovich, J. Appl. Electrochem. 29 (1999) 153–163.
[14] B. Todd, J.B. Young, J. Power Sources 110 (2002) 186.
[15] C. Cao, J. Zhang, An Introduction to Electrochemical Impedance Spectroscopy, Science Press, Beijing, 2002, pp. 37–75 (in Chinese).